PHYSICAL REVIEW D **79,** 072008 (2009)

Dalitz plot analysis of $D_s^+ \to K^+K^-\pi^+$

R. E. Mitchell,[1] M. R. Shepherd,[1] D. Besson,[2] T. K. Pedlar,[3] J. Xavier,[3] D. Cronin-Hennessy,[4] K. Y. Gao,[4] J. Hietala,[4] Y. Kubota,[4] T. Klein,[4] R. Poling,[4] A. W. Scott,[4] P. Zweber,[4] S. Dobbs,[5] Z. Metreveli,[5] K. K. Seth,[5] B. J. Y. Tan,[5] A. Tomaradze,[5] J. Libby,[6] L. Martin,[6] A. Powell,[6] C. Thomas,[6] G. Wilkinson,[6] H. Mendez,[7] J. Y. Ge,[8] D. H. Miller,[8] I. P. J. Shipsey,[8] B. Xin,[8] G. S. Adams,[9] D. Hu,[9] B. Moziak,[9] J. Napolitano,[9] K. M. Ecklund,[10] Q. He,[11] J. Insler,[11] H. Muramatsu,[11] C. S. Park,[11] E. H. Thorndike,[11] F. Yang,[11] M. Artuso,[12] S. Blusk,[12] S. Khalil,[12] R. Mountain,[12] K. Randrianarivony,[12] N. Sultana,[12] T. Skwarnicki,[12] S. Stone,[12] J. C. Wang,[12] L. M. Zhang,[12] G. Bonvicini,[13] D. Cinabro,[13] M. Dubrovin,[13] A. Lincoln,[13] M. J. Smith,[13] P. Zhou,[13] J. Zhu,[13] P. Naik,[14] J. Rademacker,[14] D. M. Asner,[15] K. W. Edwards,[15] J. Reed,[15] A. N. Robichaud,[15] G. Tatishvili,[15] E. J. White,[15] R. A. Briere,[16] H. Vogel,[16] P. U. E. Onyisi,[17] J. L. Rosner,[17] J. P. Alexander,[18] D. G. Cassel,[18] J. E. Duboscq,[18,*] R. Ehrlich,[18] L. Fields,[18] L. Gibbons,[18] R. Gray,[18] S. W. Gray,[18] D. L. Hartill,[18] B. K. Heltsley,[18] D. Hertz,[18] J. M. Hunt,[18] J. Kandaswamy,[18] D. L. Kreinick,[18] V. E. Kuznetsov,[18] J. Ledoux,[18] H. Mahlke-Krüger,[18] J. R. Patterson,[18] D. Peterson,[18] D. Riley,[18] A. Ryd,[18] A. J. Sadoff,[18] X. Shi,[18] S. Stroiney,[18] W. M. Sun,[18] T. Wilksen,[18] J. Yelton,[19] P. Rubin,[20] N. Lowrey,[21] S. Mehrabyan,[21] M. Selen,[21] and J. Wiss[21]

(CLEO Collaboration)

[1]*Indiana University, Bloomington, Indiana 47405, USA*
[2]*University of Kansas, Lawrence, Kansas 66045, USA*
[3]*Luther College, Decorah, Iowa 52101, USA*
[4]*University of Minnesota, Minneapolis, Minnesota 55455, USA*
[5]*Northwestern University, Evanston, Illinois 60208, USA*
[6]*University of Oxford, Oxford OX1 3RH, United Kingdom*
[7]*University of Puerto Rico, Mayaguez, Puerto Rico 00681*
[8]*Purdue University, West Lafayette, Indiana 47907, USA*
[9]*Rensselaer Polytechnic Institute, Troy, New York 12180, USA*
[10]*Rice University, Houston, Texas 77005, USA*
[11]*University of Rochester, Rochester, New York 14627, USA*
[12]*Syracuse University, Syracuse, New York 13244, USA*
[13]*Wayne State University, Detroit, Michigan 48202, USA*
[14]*University of Bristol, Bristol BS8 1TL, United Kingdom*
[15]*Carleton University, Ottawa, Ontario, Canada K1S 5B6*
[16]*Carnegie Mellon University, Pittsburgh, Pennsylvania 15213, USA*
[17]*Enrico Fermi Institute, University of Chicago, Chicago, Illinois 60637, USA*
[18]*Cornell University, Ithaca, New York 14853, USA*
[19]*University of Florida, Gainesville, Florida 32611, USA*
[20]*George Mason University, Fairfax, Virginia 22030, USA*
[21]*University of Illinois, Urbana-Champaign, Illinois 61801, USA*

(Received 6 March 2009; published 24 April 2009)

We perform a Dalitz plot analysis of the decay $D_s^+ \to K^+K^-\pi^+$ with the CLEO-c data set of 586 pb^{-1} of e^+e^- collisions accumulated at $\sqrt{s} = 4.17$ GeV. This corresponds to about 0.57×10^6 $D_s^{\pm}D_s^{*\mp}$ pairs from which we select 14 400 candidates with a background of roughly 15%. In contrast to previous measurements we find good agreement with our data only by including an additional $f_0(1370)\pi^+$ contribution. We measure the magnitude, phase, and fit fraction of $K^*(892)^0K^+$, $\phi(1020)\pi^+$, $K_0^*(1430)K^+$, $f_0(980)\pi^+$, $f_0(1710)\pi^+$, and $f_0(1370)\pi^+$ contributions and limit the possible contributions of other KK and $K\pi$ resonances that could appear in this decay.

DOI: 10.1103/PhysRevD.79.072008 PACS numbers: 13.25.Ft, 11.80.Et, 13.25.−k, 14.40.Lb

I. INTRODUCTION

The decay $D_s^+ \to K^+K^-\pi^+$ is among the largest known branching fractions for the D_s meson. For some time the mode $D_s^+ \to \phi(1020)\pi^+$ was used as the normalizing mode for D_s decay branching fractions, typically done by choosing events with the K^+K^- invariant mass near the narrow $\phi(1020)$ peak. Observation of a large contribution from $D_s^+ \to f_0(980)\pi^+$ [1] makes the selection of $D_s^+ \to \phi(1020)\pi^+$ dependent on the range of K^+K^- invariant

[*]Deceased.

mass chosen; the observed yield of non-ϕ contributions can be larger than 10% [2]. This is an unacceptably large uncertainty for a normalizing mode, and we proposed [2] that the branching fraction for $D_s^+ \to K^+K^-\pi^+$ in the neighborhood of the ϕ peak, without any attempt to identify the $\phi\pi^+$ component as such, could be used for D_s normalization. Relating the $D_s^+ \to K^+K^-\pi^+$ branching fraction in [2] to the rates for such phase-space-restricted subsets requires an understanding of the resonance contributions to the final state. The only published Dalitz plot (DP) analysis [3] has been done by the E687 Collaboration [1] using 701 signal events. The FOCUS Collaboration has studied this decay in a Dalitz plot analysis in an unpublished thesis [4] and a conference presentation [5].

Here we describe a Dalitz plot analysis of $D_s^+ \to K^+K^-\pi^+$ using the CLEO-c data set which yields a sample of over 12 000 signal candidates. Charge conjugation is implied throughout except where explicitly mentioned. The next section describes our experimental techniques, the third section gives our Dalitz plot analysis formalism, the fourth describes our fits to the data, and there is a brief conclusion.

II. EXPERIMENTAL TECHNIQUE

CLEO-c is a general purpose detector which includes a tracking system for measuring momenta and specific ionization of charged particles, a ring imaging Cherenkov detector to aid particle identification, and a CsI calorimeter for detection of electromagnetic showers. These components are immersed in a magnetic field of 1 T, provided by a superconducting solenoid, and surrounded by a muon detector. The CLEO-c detector is described in detail elsewhere [6].

We reconstruct the $D_s^+ \to K^+K^-\pi^+$ decay using three tracks measured in the tracking system. Charged tracks satisfy standard goodness-of-fit quality requirements [7]. Pion and kaon candidates are required to have specific ionization, dE/dx, in the main drift chamber within 4 standard deviations of the expected value at the measured momentum.

We use two kinematic variables to select $D_s^+ \to K^+K^-\pi^+$ decays, the candidate invariant mass

$$m_{\rm inv} \equiv m(K^+K^-\pi^+) \quad \text{or} \quad \Delta m_{\rm inv} = m_{\rm inv} - m_{D_s}, \quad (1)$$

and the beam constrained mass

$$m_{\rm BC} = \sqrt{E_{\rm beam}^2 - p_D^2} \quad \text{or} \quad \Delta m_{\rm BC} = m_{\rm BC} - m_{\rm BC}(D_s), \quad (2)$$

where $m_{D_s} = 1968.2\ \text{MeV}/c^2$ [8] is the D_s mass, $E_{\rm beam}$ is the beam energy, p_D is the momentum of the reconstructed D_s^+ candidate, and $m_{\rm BC}(D_s) = 2040.25\ \text{MeV}/c^2$ is the expected $m_{\rm BC}$ value of the D_s meson in the process $e^+e^- \to D_s^* D_s$ at $\sqrt{s} = 4170$ MeV. We require $|\Delta m_{\rm inv}| < 2\sigma(m_{\rm inv})$, $|\Delta m_{\rm BC}| < 2\sigma(m_{\rm BC})$, where the resolutions $\sigma(m_{\rm inv}) = 4.8\ \text{MeV}/c^2$ ($4.79 \pm 0.05\ \text{MeV}/c^2$ in single Gaussian fit) and $\sigma(m_{\rm BC}) = 2\ \text{MeV}/c^2$ ($1.89 \pm 0.02\ \text{MeV}/c^2$) represent the widths of the signal peak in the two-dimensional distribution. When there are multiple D_s-meson candidates in a single event, we select the one with the smallest $\Delta m_{\rm BC}$ value.

We use a kinematic fit to all 3-track combinations which enforces a common vertex and D_s^+ mass constraint. The kinematic fit-corrected 4-momenta of all 3 particles are used to calculate invariant masses for further Dalitz plot analysis. The resolution on the resonance invariant mass is almost always better than 5 MeV/c^2.

After all requirements, we select 14 400 candidate events for the Dalitz plot analysis. The fraction of background, 15.1%, in this sample is estimated from the fits to the $m_{\rm inv}$ spectrum shown in Fig. 1. In most fits to the Dalitz plot we constrain the value of the signal fraction, $f_{\rm sig} = 84.90 \pm 0.15\%$. In cross-checks we use a set of subsamples, splitting the data by time of observation and by the sign of D_s-meson charge, D_s^+ and D_s^-. We also consider samples with tight (1×1 standard deviations in $m_{\rm BC}$ and $m_{\rm inv}$) and loose (3×3 standard deviations) selection versus the standard selection, as well as samples of D_s mesons produced in $D_s^* \to D_s\gamma$ decays, selected with a displaced signal box using $m_{\rm BC}$ low band [$|m_{\rm BC} - 2025\ \text{MeV}/c^2| < 4\sigma(m_{\rm BC})$] and $m_{\rm BC}$ high band [$|m_{\rm BC} - 2060\ \text{MeV}/c^2| < 4\sigma(m_{\rm BC})$].

To determine the efficiency we use a signal Monte Carlo (MC) [9] simulation where one of the charged D_s mesons decays in the $KK\pi$ mode uniformly in the phase space, while the other D_s meson decays in all known modes with relevant branching fractions. In total we generated 10^6 D_s^+ and D_s^- signal decays. These underlying events are input to the CLEO-c detector simulation and processed with the CLEO-c reconstruction package. The MC-generated

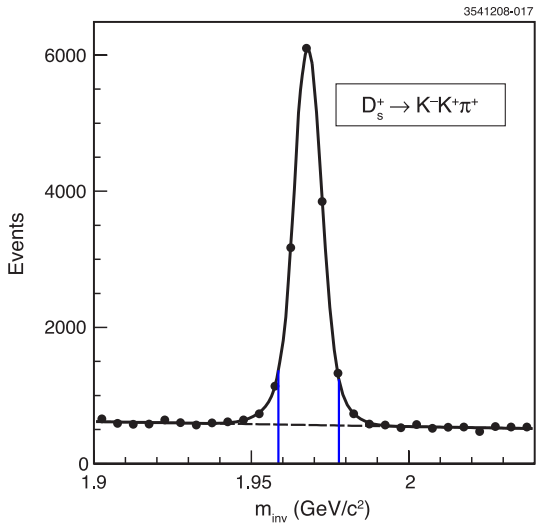

FIG. 1 (color online). The $m_{\rm inv}$ distribution. The vertical (blue online) lines show the $\pm 2\sigma$ signal region.

events are required to pass the same selection requirements as data selected in the signal box. We only select the signal-side D_s mesons which decay uniformly in the phase space, separating them by charge.

We analyze events on the Dalitz plot by choosing $x = m^2(K^+K^-)$ and $y = m^2(K^-\pi^+)$ as the independent (x, y) variables. The third variable $z = m^2(K^+\pi^+)$ is dependent on x and y through energy and momentum conservation. We do not expect any resonant substructure in the $K^+\pi^+$ invariant mass; with these Dalitz plot variables any structure in z is due to reflections of structures in x and y. Figure 2 shows the Dalitz plot. Besides the clear $\phi(1020)$ and $K^*(892)$ signal, no other narrow features are clearly observed. The variation of the population density along the resonance band clearly indicates that these resonances are spin one, as the amplitude for a spin-one resonance should have a node in the middle of its band. There is a significant population density in the node region of the $\phi(1020)$ resonance, indicating that there is likely to be an additional contribution.

To parametrize the efficiency $\varepsilon(x, y)$, we use a third-order polynomial function with respect to the arbitrary point $(x_c, y_c) = (2, 1)$ $(\mathrm{GeV}/c^2)^2$ on the Dalitz plot times threshold functions in each of the Dalitz variables to account for the loss of efficiency at the edges of the Dalitz plot, such that

$$\varepsilon(x, y) = \varepsilon_{\mathrm{poly}}(x, y)T(x)T(y)T(z(x, y)). \quad (3)$$

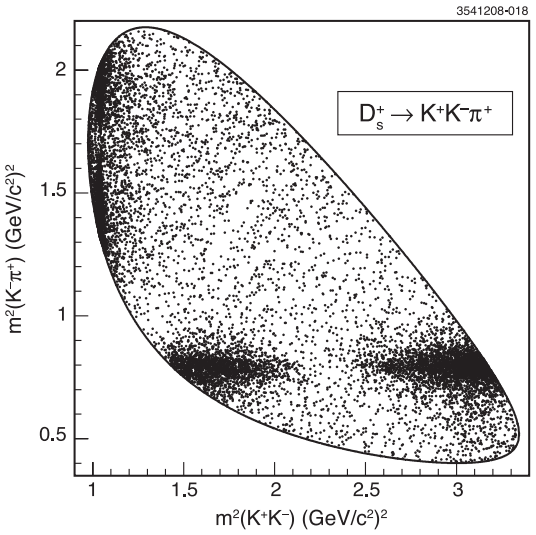

FIG. 2. The Dalitz plot for the data.

With $\hat{x} = x - x_c$ and $\hat{y} = y - y_c$, the efficiency is the product of the polynomial function

$$\varepsilon_{\mathrm{poly}}(x, y) = 1 + E_x\hat{x} + E_y\hat{y} + E_{x^2}\hat{x}^2 + E_{y^2}\hat{y}^2 + E_{x^3}\hat{x}^3 + E_{y^3}\hat{y}^3 + E_{xy}\hat{x}\,\hat{y} + E_{x^2y}\hat{x}^2\hat{y} + E_{xy^2}\hat{x}\hat{y}^2. \quad (4)$$

For each Dalitz plot variable, v ($\equiv x$, y, or z) the threshold function is sinelike with

$$T(v) = \begin{cases} [E_{c,v} + (1 - E_{c,v})] \times \sin(E_{\mathrm{th},v} \times |v - v_{\mathrm{max}}|) & \text{at } 0 < E_{\mathrm{th},v} \times |v - v_{\mathrm{max}}| < \pi/2 \\ 1 & \text{at } E_{\mathrm{th},v} \times |v - v_{\mathrm{max}}| \geq \pi/2. \end{cases} \quad (5)$$

All polynomial coefficients, E_x, E_y, E_{x^2}, E_{y^2}, E_{x^3}, E_{y^3}, E_{xy}, E_{x^2y}, E_{xy^2}, $E_{c,v}$, and $E_{\mathrm{th},v}$, are fit parameters. Each variable v has two thresholds, v_{min} and v_{max}. We expect low efficiency in the regions $v \approx v_{\mathrm{max}}$ only, where one of three particles is produced with zero momentum in the D_s-meson rest frame and thus has a small momentum in the laboratory frame.

The simulated signal sample is used to determine the efficiency. Table I shows the results of the fit to the entire signal MC sample of $D_s^+ \to K^+K^-\pi^+$ events selected on the Dalitz plot. The polynomial function with threshold factors describes the efficiency shape very well for our sample. We also fit separately the signal MC subsamples for $D_s^+ \to K^+K^-\pi^+$ and $D_s^- \to K^-K^+\pi^-$ decays, for simulations of early and late data sets, and for tight and loose signal boxes. In cross-checks with subsamples we fix the threshold parameters to their values from the central fit in order to remove correlations with other polynomial parameters. We find that the variation of the efficiency polynomial parameters is small compared to their statistical uncertainties. In fits to data we use this efficiency shape with fixed parameters, and constrained variation is allowed as a systematic check. The CLEO-c simulation for charged tracks is very well tuned, with an estimated uncertainty for the track finding efficiency of less than 0.5%. The system-

TABLE I. Fit parameters for describing the efficiency across the Dalitz plot.

Parameter	Value
E_x	0.023 ± 0.012
E_y	0.037 ± 0.014
E_{x2}	-0.307 ± 0.014
E_{xy}	-0.526 ± 0.034
E_{y2}	-0.201 ± 0.034
E_{x3}	0.262 ± 0.026
E_{x2y}	0.953 ± 0.078
E_{xy2}	0.887 ± 0.098
E_{y3}	0.004 ± 0.051
$E_{\mathrm{th},x}$	3.23 ± 0.18
$E_{\mathrm{th},y}$	2.53 ± 0.13
$E_{\mathrm{th},z}$	2.61 ± 0.13
$E_{c,x}$	0.166 ± 0.042
$E_{c,y}$	0.320 ± 0.034
$E_{c,z}$	0.338 ± 0.034

atic effect of this uncertainty on Dalitz amplitudes and derived fit fractions is negligible.

The shape for the background on the Dalitz plot is estimated using data events from an $m_{\rm BC}$ sideband region, $|m_{\rm BC} - 1900\ {\rm MeV}/c^2| < 5\sigma(m_{\rm BC})$. We only consider events from the low mass $m_{\rm BC}$ sideband, as the high mass sideband is contaminated by signal events due to initial state radiation. To parametrize the background shape on the Dalitz plot, we employ a function similar to that used for the efficiency, shown in Eq. (4). We add incoherently to the polynomial two peaking contributions to represent $K^*(892)$ and $\phi(1020)$ contributions described with Breit-Wigner functions with floating normalization coefficients, B_{K^*} and B_ϕ, respectively. Figure 3 and Table II show results of the fit to the background polynomial function for our sample. We also consider the variation of the background shape parameters for subsamples, split for D_s^+ and D_s^-, for earlier and later data sets, and for tight and loose cuts on background selection box. The variation of the shape parameters is small compared to their statistical uncertainties. Furthermore, in fits to data we use the background shape with fixed parameters, and constrained variation is allowed as a systematic cross-check. We also allow the size of the narrow resonance contributions to the background to float freely as a systematic variation. In our background model the narrow resonances have a flat decay angle distribution which is consistent with what we observe in the sideband sample and in simulation of generic D_s events. This also agrees with our expectation if the background is dominated by random combinatorics as predicted by our simulation.

TABLE II. Fit parameters for the background sample. Values in parentheses show an uncertainty or variation of the last significant digits.

Parameter	Value
B_x	-0.23 ± 0.11
B_y	0.06 ± 0.13
B_{x2}	-0.29 ± 0.12
B_{xy}	-0.99 ± 0.29
B_{y2}	-0.47 ± 0.32
B_{x3}	0.77 ± 0.23
B_{x2y}	1.98 ± 0.67
B_{xy2}	2.24 ± 0.84
B_{y3}	0.56 ± 0.47
B_ϕ	0.000 161(23)
B_{K^*}	0.001 44(28)

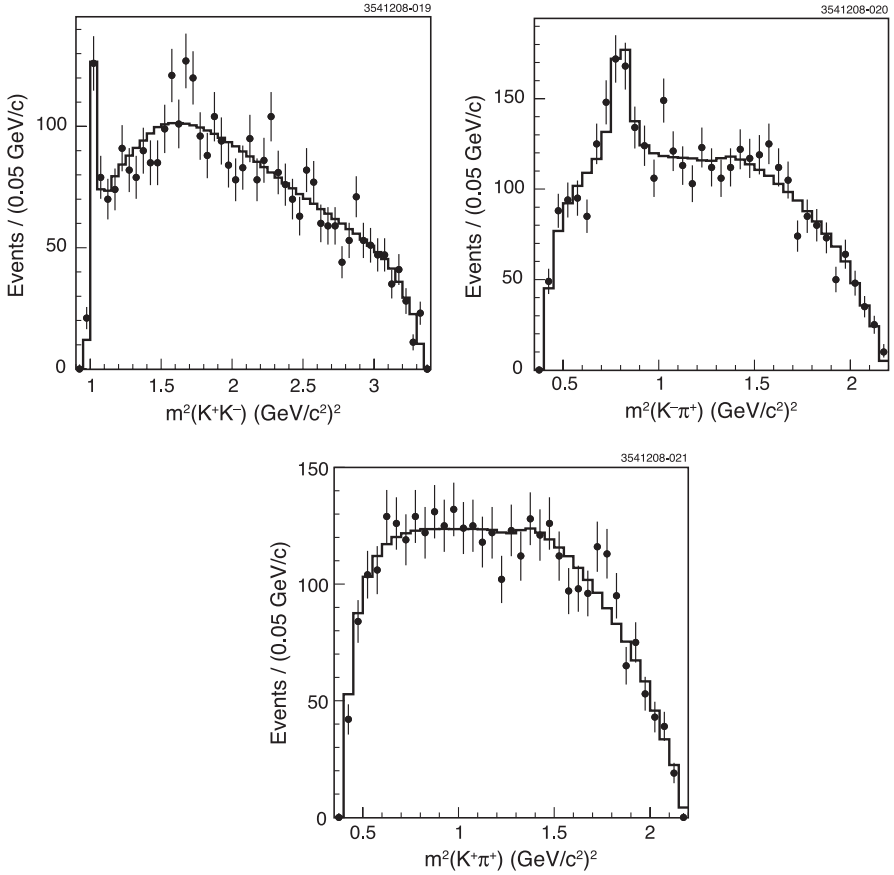

FIG. 3. Projections of the fit to the background shape described in the text (line) displayed over the data (dots) in the background box.

III. FORMALISM

This Dalitz plot analysis employs the techniques and formalism described in Ref. [10] that have been applied in many other CLEO analyses. We use an unbinned maximum likelihood fit that minimizes the sum over N events:

$$\mathcal{L} = -2\sum_{n=1}^{N} \log \mathcal{P}(x_n, y_n), \tag{6}$$

where $\mathcal{P}(x, y)$ is the probability density function (p.d.f.), which depends on the event sample being fit,

$$\mathcal{P}(x, y) = \begin{cases} \mathcal{N}_\varepsilon \varepsilon(x, y) & \text{for efficiency} \\ \mathcal{N}_B B(x, y) & \text{for background} \\ f_{\rm sig}\mathcal{N}_S |\mathcal{M}(x, y)|^2 \varepsilon(x, y) + (1 - f_{\rm sig})\mathcal{N}_B B(x, y) & \text{for signal.} \end{cases} \tag{7}$$

The shapes for the efficiency $\varepsilon(x, y)$ and background $B(x, y)$ are discussed in the previous section. The signal p.d.f. is proportional to the efficiency-corrected matrix element squared, $|\mathcal{M}(x, y)|^2$. As described above, the signal fraction $f_{\rm sig}$ is defined from the invariant mass spectrum. The background term has a relative $(1 - f_{\rm sig})$ fraction. The efficiency, signal, and background fractions are normalized separately, $1/\mathcal{N}_\varepsilon = \int \varepsilon(x, y)dxdy$, $1/\mathcal{N}_S = \int |\mathcal{M}(x, y)|^2 \varepsilon(x, y)dxdy$, $1/\mathcal{N}_B = \int B(x, y)dxdy$, which provides the overall p.d.f. normalization, $\int \mathcal{P}(x, y)dxdy = 1$. The matrix element is a sum of partial amplitudes,

$$\mathcal{M} = \sum_R c_R \times \mathcal{W}_R \times \Omega_R \times \mathcal{F}_D^L \times \mathcal{F}_R^L, \tag{8}$$

where $\mathcal{W}_R$ depends on the spin of resonance R. The factor Ω_R is the angular distribution for the resonance, and the factors $\mathcal{F}_D^L$ and $\mathcal{F}_R^L$ are the Blatt-Weisskopf angular momentum barrier-penetration factors [11]. In our standard fit the complex factor $c_R = a_R e^{i\phi_R}$ is represented by two real numbers, an amplitude a_R and a phase ϕ_R. These are included in the list of fit parameters and can be left to float freely or fixed.

Assuming the decay chain $d \to Rc \to abc$ we may write the angular distribution

$$\begin{aligned} \Omega_R^{L=0} &= 1, \\ \Omega_R^{L=1} &= m_{bc}^2 - m_{ac}^2 + \frac{(m_d^2 - m_c^2)(m_a^2 - m_b^2)}{m_{ab}^2}, \\ \Omega_R^{L=2} &= [\Omega_R^{L=1}]^2 - \frac{1}{3}\left(m_{ab}^2 - 2m_d^2 - 2m_c^2 + \frac{(m_d^2 - m_c^2)^2}{m_{ab}^2}\right)\left(m_{ab}^2 - 2m_a^2 - 2m_b^2 + \frac{(m_a^2 - m_b^2)^2}{m_{ab}^2}\right), \end{aligned} \tag{9}$$

where m_d is the mass of the decaying particle and m_a, m_b, and m_c are the masses of the daughters; m_{ab}, m_{ac}, and m_{bc} are the relevant invariant masses. These expressions for angular distributions can be obtained from covariant-tensor formalism or from orbital momentum partial wave decomposition using Legendre polynomials $P_L(\cos\theta)$, where θ is the angle between particles a and c in the resonance R rest frame.

For regular resonances such as $K^*(892)$, $\phi(1020)$, $K^*(1410)$, $K_2^*(1430)$, etc., we use the standard Breit-Wigner function

$$\mathcal{W}_R(m) = \frac{1}{m_R^2 - m^2 - im_R\Gamma(m)} \tag{10}$$

multiplied by the angular distribution Ω_L and the Blatt-Weisskopf form factors $\mathcal{F}_D^L(q)$ and $\mathcal{F}_R^L(q)$ for the D-meson and resonance R decay vertices, respectively. We assume that the mass-dependent width has the usual form

$$\Gamma(m) = \Gamma_R \frac{m_R}{m}\left(\frac{\rm P}{\rm P_R}\right)^{2L+1}[\mathcal{F}_R^L({\rm P} \times r_R)]^2, \tag{11}$$

where P is the decay products' momentum value in the decaying particle rest frame and r_R is the effective resonance radius. The form factors $\mathcal{F}_D^L(q)$ and $\mathcal{F}_R^L(q)$ in Eqs. (8) and (11) are defined in the Blatt-Weisskopf form [11]

$$L = 0\text{: } \mathcal{F}_V^0(q) = 1, \tag{12}$$

$$L = 1\text{: } \mathcal{F}_V^1(q) = \mathcal{N}_V^1 \times [1 + q^2]^{-1/2}, \tag{13}$$

$$L = 2\text{: } \mathcal{F}_V^2(q) = \mathcal{N}_V^2 \times [9 + 3q^2 + q^4]^{-1/2}, \tag{14}$$

where the label V stands for the D or R decay vertex, $q = {\rm P} \times r_V$, r_V is an effective meson radius, and $\mathcal{N}_V^L$ is a normalization constant defined by the condition $\mathcal{F}_V^L({\rm P_R} \times r_V) = 1$, where $\rm P_R$ is the products' momentum value at $m = m_R$.

The $\mathcal{W}_R$ parametrization of the $f_0(980)$, whose mass m_{f_0} is close to the $K\bar{K}$ production threshold, uses the Flatté [12] formula

$$\mathcal{W}_R(m) = \frac{1}{m_R^2 - m^2 - i\sum_{ab} g_{Rab}^2 \rho_{ab}(m)} \tag{15}$$

where ab stands for $\pi^0\pi^0$, $\pi^+\pi^-$, K^+K^-, and $K^0\bar{K}^0$, and $\rho_{ab}(m) = 2{\rm P}_a/m$ is a phase space factor, calculated for the decay products' momentum $\rm P_a$ in the resonance rest frame. We use the following isospin relations for the coupling constants: $g_{f_0\pi^+\pi^-} = \sqrt{2/3}g_{f_0\pi\pi}$, $g_{f_0\pi^0\pi^0} = \sqrt{1/3}g_{f_0\pi\pi}$,

TABLE III. Parameters of contributing resonances.

Resonance	J^{PC}	Mass (MeV/c^2)	Width (MeV/c^2)
$K\pi$ states			
$K^*(892)$	1^-	896.00 ± 0.25	50.3 ± 0.6
$K^*(1410)$	1^-	1414 ± 15	232 ± 21
$K_0^*(1430)$	0^+	1414 ± 6	290 ± 21
$K_2^*(1430)$	2^+	1432.4 ± 1.3	109 ± 5
$K^*(1680)$	1^-	1717 ± 27	322 ± 110
κ	0^+	Re $m = 710$	Im $m = -310$
K^+K^- states			
$f_0(980)$	0^{++}	965 ± 10	$g_{\pi\pi} = 406$ $g_{KK} = 800$
$a_0(980)$	0^{++}	999 ± 1	$g_{\eta\pi} = 620$ $g_{KK} = 500$
$\phi(1020)$	1^{--}	1019.460 ± 0.019	4.26 ± 0.05
$f_2(1270)$	2^{++}	1275.4 ± 1.1	$185.2^{+3.1}_{-2.5}$
$a_2(1320)$	2^{++}	1318.3 ± 0.6	107 ± 5
$f_0(1370)$	0^{++}	1200 to 1500	200 to 500
$a_0(1450)$	0^{++}	1474 ± 19	265 ± 13
$f_0(1500)$	0^{++}	1507 ± 5	109 ± 7
$f_2(1525)$	2^{++}	1525 ± 5	73^{+6}_{-5}
$f_0(1710)$	0^{++}	1718 ± 6	137 ± 8
$\phi(1680)$	1^{--}	1680 ± 20	150 ± 50

and $g_{f_0K^0\bar{K}^0} = g_{f_0K^+K^-} = \sqrt{1/2}g_{f_0K\bar{K}}$. Their values, shown in Table III, are taken from the BES experiment [13].

We model a low mass $K^+\pi^-$ S wave, also known as κ or $K(800)$, using a complex pole amplitude proposed in Ref. [14],

$$\mathcal{W}_\kappa(m) = \frac{1}{m_\kappa^2 - m^2}, \tag{16}$$

where $m_\kappa = (0.71 - i0.32)$ GeV is a pole position in the complex $s = m^2(K^+\pi^-)$ plane estimated from the results of several experiments.

In this analysis we use or test all known $K^-\pi^+$ and K^+K^- resonances recognized by the Particle Data Group (PDG) [8] which can be observed in the phase space of the $D_s^+ \to K^-K^+\pi^+$ decay. These are listed in Table III. One could expect a contribution in the K^+K^- mass spectrum from the $f_0(980)$ and $a_0(980)$ scalar resonances. Their K^+K^- mass spectra have similar, but not well-defined shapes. If both amplitudes are allowed to float simultaneously in the fit, they show a huge destructive interference, which is sensitive to their shape parameters. The $f_0(980)$ contribution dominates [8] in the $D_s^+ \to \pi^+\pi^+\pi^-$ decay, which has a large branching fraction, $\mathcal{B}(D_s^+ \to \pi^+\pi^+\pi^-) = (1.22 \pm 0.23)\%$. The relevant coupled channel of the $a_0(980)$ has not been observed in the $D_s^+ \to \eta\pi^0\pi^+$ decay. In this analysis we consider the $f_0(980)$ contribution only.

IV. FITS TO DATA

First, we analyze our data with the model used by E687 [1]. Their isobar model contains five contributions, $K^*(892)^0K^+$, $\phi(1020)\pi^+$, $K_0^*(1430)K^+$, $f_0(980)\pi^+$, and $f_0(1710)\pi^+$. In our analysis of $D^+ \to K^-\pi^+\pi^+$ and $D^+ \to K^-K^+\pi^+$ decays we find a $K^*(892)$ width that is smaller than the world average value from the PDG [8]. Thus we let the mass and width of $K^*(892)$ float in the fit. Results are shown in Table IV. In this table and all succeeding tables, the units of the amplitudes are arbitrary (a.u.). We find that the sign of the $\phi(1020)$ contribution is opposite to the sign obtained by E687, but all other results are consistent within quoted uncertainties. We find that this fit to our data sample has a poor χ^2/ν, where ν is the number of degrees of freedom, giving a very small fit probability. The χ^2 is calculated over adaptive bins, similar to our previous analysis [15]. This model does not represent our data well, especially in the range of $1.1 < m_{KK}^2 < 1.5$ GeV$^2/c^4$.

The E687 model contains five resonances. Two of them, $K^*(892)$ and $\phi(1020)$, are clearly seen on the Dalitz plot. The other three, $K_0^*(1430)$, $f_0(980)$, and $f_0(1710)$, are too wide to be easily discerned. To check their significance we remove them one by one from the total amplitude and check the fit results. In all fits where we remove one resonance the fit quality is degraded, increasing χ^2/ν by more than 0.6, compared to our central fit. Thus, we assume that all five resonances from the E687 model are significant.

In order to get better consistency between the model and data, we try to improve the E687 model by adding contributions from the other known resonances listed in Table III. The results of these fits are shown in Tables V and VI as a variation of the fit parameters with respect to the central case. In all cases the fit quality is improved and each additional resonance has a significant magnitude. We conclude that the five-resonance model based on the E687 results does not fully describe the data sample. The largest fit quality improvement is achieved in the case of additional S-wave contributions: $f_0(1370)$, nonresonant (NR), $a_0(1450)$, and κ. Adding the $f_0(1370)$ contribution gives the largest improvement of the fit quality, $\Delta\chi^2 = -100$, for two fewer degrees of freedom.

We consider a six-resonance model, called model A, containing $K^*(892)^0K^+$, $\phi(1020)\pi^+$, $K_0^*(1430)K^+$, $f_0(980)\pi^+$, $f_0(1710)\pi^+$, and $f_0(1370)\pi^+$ contributions. Model A is simply the E687 isobar model with an additional $f_0(1370)\pi^+$ contribution. Results with this model and fit projections are shown in Fig. 4. We repeat the previous procedure and include an additional resonance and check the significance of its parameters and consistency of the p.d.f. with our data sample. Results are shown in Tables VII and VIII. For model A we do not find any additional resonances with significant magnitude, the fit quality does not significantly improve, and thus we take

TABLE IV. Comparison of CLEO-c results with E687 using the E687 isobar model. Shown are the fitted magnitudes, a in arbitrary units, the phases (ϕ) in degrees, defined relative to the $K^*(892)^0\pi^+$ amplitude, and the fit fractions (FF).

Mode	Parameter	E687	CLEO-c (PDG)
$\bar{K}^*(892)^0K^+$	a	(fixed)	1 (fixed)
	ϕ (°)	0 (fixed)	0 (fixed)
	m (MeV/c^2)		895.8 ± 0.5 [896.00 ± 0.25]
	Γ (MeV/c^2)		44.2 ± 1.0 [50.3 ± 0.06]
	FF (%)	47.8 ± 4.6 ± 4.0	48.2 ± 1.2
$\bar{K}_0^*(1430)K^+$	a	···	1.76 ± 0.12
	ϕ (°)	152 ± 40 ± 39	145 ± 8
	FF (%)	9.3 ± 3.2 ± 3.2	5.3 ± 0.7
$\phi(1020)\pi^+$	a	···	1.15 ± 0.02
	ϕ (°)	178 ± 20 ± 24	−15 ± 4
	FF (%)	39.6 ± 3.3 ± 4.7	42.7 ± 1.3
$f_0(980)\pi^+$	a	···	3.67 ± 0.13
	ϕ (°)	159 ± 22 ± 16	156 ± 3
	FF (%)	11.0 ± 3.5 ± 2.6	16.8 ± 1.1
$f_0(1710)\pi^+$	a	···	1.27 ± 0.07
	ϕ (°)	110 ± 20 ± 17	102 ± 4
	FF (%)	3.4 ± 2.3 ± 3.5	4.4 ± 0.4
$\sum$ FF (%)		111.1	117.3 ± 2.2
Number of events on DP			14 400
Number of signal events		701 ± 36	12 226 ± 22
Goodness	χ^2/ν	50.2/33	278/119

this model for our central result. For each additional resonance we estimate an upper limit on its fit fraction at the 90% confidence level, as also shown in Tables VII and VIII. We conclude that the six-resonance model A p.d.f. gives a good description of our data sample.

For model A we test the resonance shape parameters by floating the mass and width, or two coupling constants in the case of $f_0(980)$, for each resonance. Results of these fits are shown in Tables IX and X. We find that all parameters are consistent with their central fit values used in the fit with model A.

To estimate systematic uncertainties of the fit parameters, we apply numerous variations to the fitting procedure and look at the change of the fit parameters from the central result. We consider subsamples where the data are split into earlier and later data sets, and D_s^+ and D_s^- decays, and are selected using tight and loose signal boxes. These are shown in Table XI. These results are obtained with fixed

TABLE V. Fits to CLEO-c data using the E687 model with additional $K^-\pi^+$ resonances. For the contributions that do not change, the entries in the table are changes from the E687 model.

Parameter	E687 model	Nonresonant	$K^*(1410)$	$K_2^*(1430)$	$K^*(1680)$	κ
$m_{K^*(892)}$	895.8 ± 0.5	0.0	−0.4	−0.1	−1.2	−0.9
$\Gamma_{K^*(892)}$	44.2 ± 1.0	0.4	−1.3	0.3	−2.1	−0.3
$a_{K_0^*(1430)}$ (a.u.)	1.76 ± 0.12	−1.16	−0.02	0.14	0.05	−0.58
$\phi_{K_0^*(1430)}$ (°)	145 ± 8	−4.2	4	7.3	−4	−7
$a_{f_0(980)}$ (a.u.)	3.67 ± 0.13	1.64	0.28	−0.19	0.69	0.91
$\phi_{f_0(980)}$ (°)	156 ± 3	41	−2.2	4.3	−0.78	29
$a_{\phi(1020)}$ (a.u.)	1.15 ± 0.02	−0.02	0.04	0.003	0.06	−0.01
$\phi_{\phi(1020)}$ (°)	−15 ± 4	32	−13	0.6	−10.4	26
$a_{f_0(1710)}$ (a.u.)	1.27 ± 0.07	−0.83	0.06	−0.07	0.22	−0.87
$\phi_{f_0(1710)}$ (°)	102 ± 4	−27	−9.4	3.0	−6.7	−15
a_{add} (a.u.)		5.2 ± 0.4	1.77 ± 0.21	0.92 ± 0.15	6.3 ± 0.9	2.27 ± 0.17
ϕ_{add} (°)		193 ± 4	93 ± 6	−179 ± 16	117 ± 9	51 ± 4
χ^2/ν	278/119	192/117	249/117	241/117	256/117	200/117

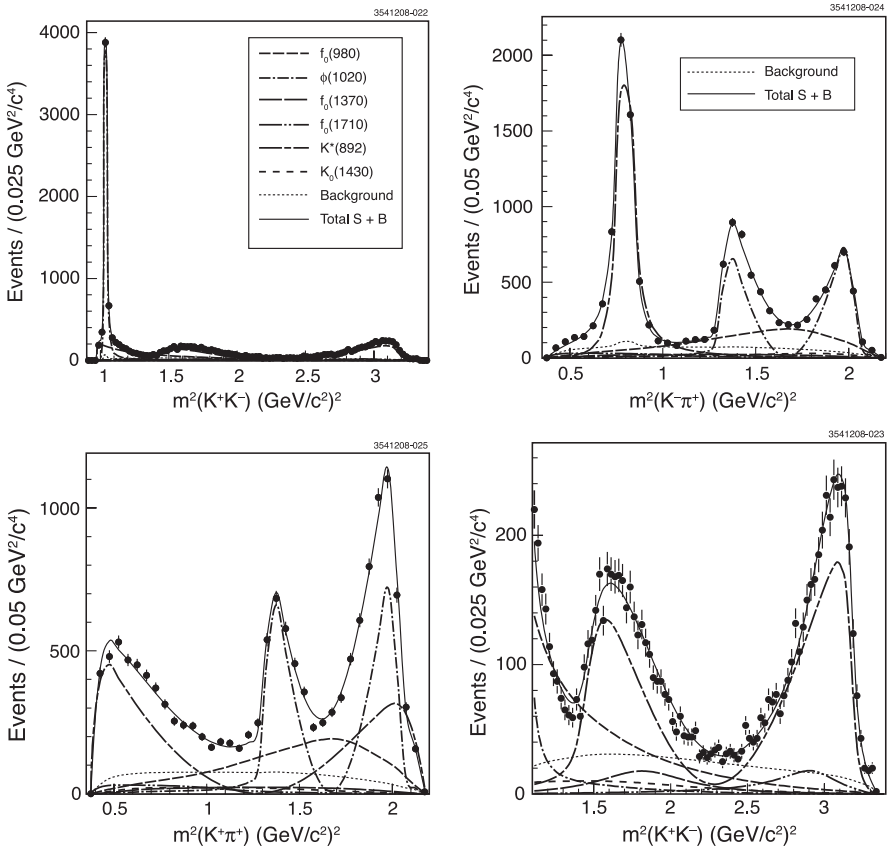

FIG. 4. Fit to data for model A, and projections of the Dalitz plot. The final plot shows the $m^2(KK)$ projection of the Dalitz plot for values of $m^2(KK)$ larger than the contribution from the $\phi(1020)$.

parameters for efficiency and background functions from Tables I and II. We also consider fits with floating efficiency or background parameters in Table XII. In these fits all polynomial coefficients for the efficiency or background, including resonance background amplitudes, float freely, but we fit simultaneously two samples of events for data plus the signal MC efficiency or background box to constrain the variation of the efficiency or background parameters. We also fit allowing the signal fraction to float, and find $f_{\rm sig} = 0.8495 \pm 0.0070$ which is consistent with 0.8490 used in the central fit.

TABLE VI. Fits to CLEO-c data using the E687 model with additional K^+K^- resonances. For the contributions that do not change, the entries in the table are changes from the E687 model.

Parameter	E687 model	$f_2(1270)$	$a_2(1320)$	$f_0(1370)$	$f_0(1500)$	$f_2(1525)$	$a_0(1450)$	$\phi(1680)$
$m_{K^*(892)}$	895.8 ± 0.5	−0.4	−0.1	−0.9	−0.5	0.0	−0.8	0.1
$\Gamma_{K^*(892)}$	44.2 ± 1.0	2.3	2.4	1.5	0.6	0.6	1.0	1.2
$a_{K_0^*(1430)}$ (a.u.)	1.76 ± 0.12	0.11	0.08	−0.25	−0.03	−0.16	−0.22	−0.18
$\phi_{K_0^*(1430)}$ (°)	145 ± 8	−32	−28	1.0	−15	1.7	−15	18
$a_{f_0(980)}$ (a.u.)	3.67 ± 0.13	0.29	0.26	1.05	0.52	0.03	1.09	0.20
$\phi_{f_0(980)}$ (°)	156 ± 3	−2	−1.6	1.3	2.3	0.22	3.8	10.5
$a_{\phi(1020)}$ (a.u.)	1.15 ± 0.02	−0.03	−0.04	−0.02	−0.003	−0.02	−0.007	−0.012
$\phi_{\phi(1020)}$ (°)	−15 ± 4	−7	−6.3	7.2	−0.6	1.5	4.3	13.2
$a_{f_0(1710)}$ (a.u.)	1.27 ± 0.07	0.08	0.07	−0.16	0.17	−0.04	0.03	−0.018
$\phi_{f_0(1710)}$ (°)	102 ± 4	7	4.7	−13	−4.1	−3.8	−17	5.3
$a_{\rm add}$ (a.u.)		0.64 ± 0.09	0.45 ± 0.06	1.15 ± 0.09	0.50 ± 0.05	0.50 ± 0.07	1.32 ± 0.10	1.04 ± 0.17
$\phi_{\rm add}$ (°)		17 ± 9	40 ± 8	53 ± 5	132 ± 7	173 ± 10	103 ± 5	−4 ± 11
χ^2/ν	278/119	237/117	237/117	178/117	229/117	249/117	192/117	256/117

TABLE VII. Fits to data using model A with additional nonresonant contributions or $K^+\pi^-$ resonance. For the contributions that do not change, the entries in the table are changes from model A.

Parameter	Model A	NR	$K^*(1410)$	$K_2^*(1430)$	$K^*(1680)$	κ
$m_{K^*(892)}$	894.9 ± 0.5	0.3	0.1	0.2	0.2	-0.1
$\Gamma_{K^*(892)}$	45.7 ± 1.1	-0.1	0.1	0.8	0.6	-0.3
$a_{K_0^*(1430)}$ (a.u.)	1.51 ± 0.11	-0.1878	-0.0245	0.0603	-0.1434	0.2685
$\phi_{K_0^*(1430)}$ (°)	146 ± 8	-10.833	0.4446	-4.8755	2.3676	-7.6608
$a_{f_0(980)}$ (a.u.)	4.72 ± 0.18	-0.0529	0.0057	0.2566	-0.2530	-0.2078
$\phi_{f_0(980)}$ (°)	157 ± 3	8.1153	-0.7457	1.0875	1.7545	-4.5506
$a_{\phi(1020)}$ (a.u.)	1.13 ± 0.02	-0.0005	-0.0001	-0.0096	-0.0159	0.0047
$\phi_{\phi(1020)}$ (°)	-8 ± 4	3.9973	-0.1144	-4.8349	5.2172	-5.0235
$a_{f_0(1370)}$ (a.u.)	1.15 ± 0.09	-0.0979	-0.0055	0.0535	0.0103	0.0890
$\phi_{f_0(1370)}$ (°)	53 ± 5	5.5500	-1.6829	-4.4427	3.2688	-11.386
$a_{f_0(1710)}$ (a.u.)	1.11 ± 0.07	-0.1502	-0.0093	-0.0157	-0.0442	-0.0940
$\phi_{f_0(1710)}$ (°)	89 ± 5	-7.3126	-1.2087	3.7678	2.4526	-6.2195
a_{add} (a.u.)	0	1.3 ± 0.6	0.10 ± 0.13	1.00 ± 0.26	2.18 ± 1.33	0.50 ± 0.18
ϕ_{add} (°)	0	-147 ± 19	-3 ± 119	105 ± 11	-72 ± 13	163 ± 25
FF_{add} (%)	0	1.5 ± 1.4	0.01 ± 0.03	0.40 ± 0.22	0.30 ± 0.44	0.40 ± 0.32
FF_{add} (%) @ 90% C.L.	0	$<3.3\%$	$<0.05\%$	$<0.7\%$	$<0.9\%$	$<0.8\%$
FF$[K^*(892)]$ (%)	47.4 ± 1.5	47.5	47.5	47.8	48.3	47.5
FF$[K_0^*(1430)]$ (%)	3.9 ± 0.5	3.0	3.8	4.4	3.3	5.5
FF$[f_0(980)]$ (%)	28.2 ± 1.9	27.7	28.4	32.3	26.2	25.7
FF$[\phi(1020)]$ (%)	42.2 ± 1.6	41.9	42.1	42.3	42.1	42.1
FF$[f_0(1370)]$ (%)	4.3 ± 0.6	3.5	4.2	4.8	4.5	4.9
FF$[f_0(1710)]$ (%)	3.4 ± 0.5	2.6	3.4	3.4	3.3	2.9
$\sum_R \text{FF}_R$ (%)	129.5	127.8	129.4	135.4	127.9	129.0
χ^2/ν	178/117	174/115	177/115	170/115	175/115	173/115

TABLE VIII. Fits using model A with additional K^+K^- resonance. For the contributions that do not change, the entries in the table are changes from model A.

Parameter	Model A	$f_2(1270)$	$a_2(1320)$	$f_0(1500)$	$f_2(1525)$	$a_0(1450)$	$\phi(1680)$
$m_{K^*(892)}$	894.9 ± 0.5	-0.5	-0.3	-0.1	-0.2	-0.1	-0.1
$\Gamma_{K^*(892)}$	45.7 ± 1.1	1.2	1.2	-0.1	0.2	-0.1	-0.2
$a_{K_0^*(1430)}$ (a.u.)	1.51 ± 0.11	-0.0518	-0.0587	-0.0060	-0.0822	-0.0210	-0.0152
$\phi_{K_0^*(1430)}$ (°)	146 ± 8	-13.610	-7.5258	1.1483	0.1662	2.4740	-0.8833
$a_{f_0(980)}$ (a.u.)	4.72 ± 0.18	0.0864	-0.0037	0.0521	-0.0239	0.1123	0.0113
$\phi_{f_0(980)}$ (°)	157 ± 3	-0.6746	-0.6856	0.6617	-0.3009	1.1151	-0.1360
$a_{\phi(1020)}$ (a.u.)	1.13 ± 0.02	-0.0105	-0.0126	0.0058	-0.0058	0.0068	0.0056
$\phi_{\phi(1020)}$ (°)	-8 ± 4	-2.1292	-1.5385	0.5046	-0.1244	1.2202	-0.4788
$a_{f_0(1370)}$ (a.u.)	1.15 ± 0.09	-0.0176	-0.0343	0.0336	-0.0168	0.0150	-0.0039
$\phi_{f_0(1370)}$ (°)	53 ± 5	1.0892	-0.3964	3.8125	1.4021	14.6004	0.3390
$a_{f_0(1710)}$ (a.u.)	1.11 ± 0.07	0.0041	-0.0165	-0.0161	-0.0100	-0.0533	0.0007
$\phi_{f_0(1710)}$ (°)	89 ± 5	4.7785	2.7846	-1.9584	-2.2626	-3.6665	-0.9276
a_{add} (a.u.)	0	0.40 ± 0.09	0.26 ± 0.06	0.07 ± 0.04	0.23 ± 0.08	0.37 ± 0.28	0.10 ± 0.16
ϕ_{add} (°)	0	22 ± 14	51 ± 15	37 ± 66	180 ± 26	24 ± 17	-93 ± 122
FF_{add} (%)	0	0.24 ± 0.11	0.20 ± 0.09	0.04 ± 0.10	0.09 ± 0.05	0.38 ± 0.60	0.008 ± 0.031
FF_{add} (%) @ 90% C.L.	0	$<0.4\%$	$<0.3\%$	$<0.17\%$	$<0.16\%$	$<1.2\%$	$<0.05\%$
FF$[K^*(892)]$ (%)	47.4 ± 1.5	47.2	47.4	47.3	48.0	47.3	47.4
FF$[K_0^*(1430)]$ (%)	3.9 ± 0.5	3.8	3.7	3.9	3.6	3.8	3.8
FF$[f_0(980)]$ (%)	28.2 ± 1.9	30.0	29.0	28.8	28.4	29.4	28.2
FF$[\phi(1020)]$ (%)	42.2 ± 1.6	42.1	42.2	42.2	42.1	42.2	42.1
FF$[f_0(1370)]$ (%)	4.3 ± 0.6	4.2	4.1	4.5	4.2	4.3	4.2
FF$[f_0(1710)]$ (%)	3.4 ± 0.5	3.5	3.4	3.3	3.4	3.1	3.4
$\sum_R \text{FF}_R$ (%)	129.5	131.1	130.2	130.0	129.8	130.5	129.3
χ^2/ν	178/117	169/115	170/115	177/115	172/115	176/115	178/115

TABLE IX. Optimal resonance parameters. The uncertainties for the CLEO-c results are statistical only.

Resonance	Parameter (MeV/c^2)	Central fit	Floated	PDG [8]
$K^*(892)$	m	895.8 ± 0.5	895.8 ± 0.5	896.00 ± 0.25
	Γ	44.2 ± 1.0	44.2 ± 1.0	50.3 ± 0.6
$K_0^*(1430)$	m	1414	1422 ± 23	1414 ± 6
	Γ	290	239 ± 48	290 ± 21
$f_0(980)$	m	965	933 ± 21	980 ± 10
	$g_{\pi\pi}$	406	393 ± 36	$\Gamma = 40$ to 100
	g_{KK}	800	557 ± 88	
$\phi(1020)$	m	1019.460	1019.64 ± 0.05	1019.460 ± 0.019
	Γ	4.26	4.780 ± 0.14	4.26 ± 0.05
$f_0(1370)$	m	1350	1315 ± 34	1200 to 1500
	Γ	265	276 ± 39	200 to 500
$f_0(1710)$	m	1718	1749 ± 12	1718 ± 6
	Γ	137	175 ± 29	137 ± 8

We estimate a systematic uncertainty of the model A fit parameters by combining the fit results from Tables VII, VIII, X, XI, and XII. None of the systematic variations dominate the uncertainty. The systematic uncertainty is estimated as the mean change from the central fit result, δMean, added in quadrature to the RMS of all variations. The resulting systematic uncertainties on the parameters are given in Table XIII.

V. CONCLUSION

We perform a Dalitz plot analysis of the $D_s^+ \to K^+K^-\pi^+$ decay with the CLEO-c data set of 586 pb^{-1} of e^+e^- collisions accumulated at $\sqrt{s} = 4.17$ GeV. This corresponds to about 0.57×10^6 $D_s^+ D_s^{*-}$ pairs from which we select 14 400 candidate events with a background of 15%. We compare our results with the previous measurement from E687 using the isobar model and find good agreement with the E687 parameters, as shown in Table IV. We find that all resonances from the E687 model are significant and their exclusion degrades the fit quality.

However, the fit quality is significantly improved if we add an additional K^+K^- resonance to the model. As shown in Tables V and VI, almost any additional resonance or nonresonant contribution improves the agreement with the

TABLE X. Fits to data using model A with floating resonance parameters. After the first column of data the entries in the table are changes from model A when the parameters of resonance at the top of the column are allowed to float.

Parameter	Model A	$K^*(1430)$	$f_0(980)$	$\phi(1020)$	$f_0(1370)$	$f_0(1710)$
$m_{K^*(892)}$	894.9 ± 0.5	-0.1	0	0.2	-0.1	0.1
$\Gamma_{K^*(892)}$	45.7 ± 1.1	-0.1	0.2	0.1	0.0	-0.5
$a_{K_0^*(1430)}$ (a.u.)	1.51 ± 0.11	-0.1449	-0.1527	0.0256	0.0533	-0.0305
$\phi_{K_0^*(1430)}$ (°)	146 ± 8	8.6060	-3.2558	10.2102	7.5225	-5.6685
$a_{f_0(980)}$ (a.u.)	4.72 ± 0.18	-0.0576	-0.3873	-0.3073	-0.0540	0.1767
$\phi_{f_0(980)}$ (°)	157 ± 3	-1.1202	-13.584	0.0037	-1.2207	3.4058
$a_{\phi(1020)}$ (a.u.)	1.13 ± 0.02	0.0058	-0.0018	0.0786	0.0037	0.0167
$\phi_{\phi(1020)}$ (°)	-8 ± 4	-0.8216	5.2291	1.5697	0.9613	1.3374
$a_{f_0(1370)}$ (a.u.)	1.15 ± 0.09	0.0473	-0.0319	-0.0508	0.0293	-0.1248
$\phi_{f_0(1370)}$ (°)	53 ± 5	-2.5387	4.8538	-2.6304	-17.247	3.0673
$a_{f_0(1710)}$ (a.u.)	1.11 ± 0.07	-0.0060	-0.0096	-0.0291	-0.0656	0.4223
$\phi_{f_0(1710)}$ (°)	89 ± 5	-1.9306	-1.2058	-2.4148	0.0913	20.0144
FF[$K^*(892)$] (%)	47.4 ± 1.5	47.3	47.2	47.4	47.5	46.8
FF[$K_0^*(1430)$] (%)	3.9 ± 0.5	3.8	3.2	4.1	4.2	3.7
FF[$f_0(980)$] (%)	28.2 ± 1.9	27.5	29.7	24.8	27.7	29.7
FF[$\phi(1020)$] (%)	42.2 ± 1.6	42.2	41.8	43.3	42.2	42.0
FF[$f_0(1370)$] (%)	4.3 ± 0.6	4.6	4.0	3.9	4.4	3.3
FF[$f_0(1710)$] (%)	3.4 ± 0.5	3.4	3.4	3.3	3.0	4.1
$\sum_R \mathrm{FF}_R$ (%)	129.5	128.8	129.2	126.8	129.0	129.5
χ^2/ν	178/117	177/115	169/114	168/115	176/115	166/115

TABLE XI. Fits to a variety of data samples using model A with central efficiency and background. After the first column of data the entries in the table are changes from model A with the variation indicated at the top of the column.

Variation parameter	Central fit, model A	Early data	Late data	Only D_s^+	Only D_s^-	Tight $1\sigma \times 1\sigma$	Loose $3\sigma \times 3\sigma$	Low sideband	High sideband
$m_{K^*(892)}$	894.9 ± 0.5	−0.4	3.0	−0.7	0.7	−0.2	0.2	−1.2	−1.4
$\Gamma_{K^*(892)}$	45.7 ± 1.1	0.1	0.0	−0.8	0.8	−0.2	1.0	4.8	2.2
$a_{K_0^*(1430)}$ (a.u.)	1.51 ± 0.11	0.0138	0.0177	−0.0023	0.0398	−0.0205	−0.1276	−0.8084	0.7309
$\phi_{K_0^*(1430)}$ (°)	146 ± 8	−10.971	9.7985	−17.161	17.257	−6.2148	14.408	18.400	−66.057
$a_{f_0(980)}$ (a.u.)	4.72 ± 0.18	0.3277	−0.3513	0.0484	−0.0416	−0.0364	0.0244	0.6752	0.3610
$\phi_{f_0(980)}$ (°)	157 ± 3	−1.3604	1.1808	−6.3697	6.6295	−4.5506	2.8515	3.1875	−23.699
$a_{\phi(1020)}$ (a.u.)	1.13 ± 0.02	0.0053	0.0008	0.0084	0.0011	0.0153	−0.0049	0.0079	0.0210
$\phi_{\phi(1020)}$ (°)	−8 ± 4	−2.9134	2.2119	−8.3156	8.5410	−7.0696	5.5073	8.5766	−35.140
$a_{f_0(1370)}$ (a.u.)	1.15 ± 0.09	0.0976	−0.1031	−0.0131	0.0250	−0.1193	0.1395	0.5111	0.3938
$\phi_{f_0(1370)}$ (°)	53 ± 5	−2.8318	2.2204	−4.6088	2.4167	−6.5716	−1.3470	−14.394	−28.267
$a_{f_0(1710)}$ (a.u.)	1.11 ± 0.07	0.0786	−0.0830	−0.0412	0.0483	0.0403	0.0070	0.1877	−0.3847
$\phi_{f_0(1710)}$ (°)	89 ± 5	−3.3881	2.2247	0.1313	−0.5966	0.7797	2.6467	16.146	−5.0150
FF[$K^*(892)$] (%)	47.4 ± 1.5	47.2	47.7	47.9	46.7	47.2	46.8	43.4	48.0
FF[$K_0^*(1430)$] (%)	3.9 ± 0.5	4.0	4.1	3.9	4.2	3.8	3.3	0.9	8.3
FF[$f_0(980)$] (%)	28.2 ± 1.9	32.1	24.4	28.6	27.9	27.6	28.8	37.6	31.5
FF[$\phi(1020)$](%)	42.2 ± 1.6	42.0	42.3	42.1	42.2	42.7	42.0	43.3	41.8
FF[$f_0(1370)$](%)	4.3 ± 0.6	5.0	3.5	4.1	4.5	3.4	5.4	9.0	7.4
FF[$f_0(1710)$] (%)	3.4 ± 0.5	3.9	3.0	3.2	3.8	3.7	3.5	4.8	1.4
$\sum_R \mathrm{FF}_R$ (%)	129.5	134.2	124.9	129.7	129.2	128.3	129.9	138.9	138.4
χ^2/ν	178/117	134/117	203/117	166/117	123/117	155/117	201/117	140/117	138/117
Events on DP	14400	7334	7066	7233	7167	7200	19177	6682	7232
f_{sig}	0.8490	0.8518	0.8466	0.8496	0.8497	0.9238	0.7484	0.4338	0.5696

TABLE XII. Fits to data using model A with floating efficiency and background coefficients, fits with floating f_{sig}, and fits with floating background coefficients B_{K^*} and B_ϕ for the narrow resonance contributions to the background. After the first column of data, the entries in the table are changes from model A with the variation indicated at the top of the column.

Parameter	Model A	Float E_i	Float B_i	Float f_{sig}
$m_{K^*(892)}$	894.9 ± 0.5	0	0.1	0
$\Gamma_{K^*(892)}$	45.7 ± 1.1	0	−0.2	0
$a_{K_0^*(1430)}$ (a.u.)	1.51 ± 0.11	−0.0018	−0.0121	0.0023
$\phi_{K_0^*(1430)}$ (°)	146 ± 8	0.1630	−1.6971	0.2116
$a_{f_0(980)}$ (a.u.)	4.72 ± 0.18	−0.0026	−0.0332	−0.0043
$\phi_{f_0(980)}$ (°)	157 ± 3	0.3362	−0.6851	0.2704
$a_{\phi(1020)}$ (a.u.)	1.13 ± 0.02	0.0034	−0.0007	0.0028
$\phi_{\phi(1020)}$ (°)	−8 ± 4	0.1282	−0.9907	−0.0391
$a_{f_0(1370)}$ (a.u.)	1.15 ± 0.09	−0.0015	0.0112	0.0006
$\phi_{f_0(1370)}$ (°)	53 ± 5	0.1323	−0.5403	0.0792
$a_{f_0(1710)}$ (a.u.)	1.11 ± 0.07	−0.0007	−0.0539	−0.0038
$\phi_{f_0(1710)}$ (°)	89 ± 5	−0.2072	−1.1088	−0.3882
FF[$K^*(892)$] (%)	47.4 ± 1.5	47.4	47.7	47.4
FF[$K_0^*(1430)$] (%)	3.9 ± 0.5	3.9	3.9	3.9
FF[$f_0(980)$] (%)	28.2 ± 1.9	28.2	28.1	28.2
FF[$\phi(1020)$] (%)	42.2 ± 1.6	42.2	42.2	42.2
FF[$f_0(1370)$] (%)	4.3 ± 0.6	4.2	4.4	4.3
FF[$f_0(1710)$] (%)	3.4 ± 0.5	3.4	3.1	3.4
$\sum_R \mathrm{FF}_R$ (%)	129.5	129.4	129.3	129.4
χ^2/ν	178/117	679/562	270/188	178/116

TABLE XIII. Summary of systematic cross-checks for model A. Fit parameters are shown with their statistical and systematic uncertainties, respectively. "δMean" and "RMS" account for variation of the fit parameters in the systematic cross-checks as discussed in the text. "Total" is a quadratic sum of δMean and RMS, and after rounding it is the systematic uncertainty given in the second column. The results of the E687 model are also shown for comparison.

Parameter	Model A	δMean	RMS	Total	E687 model
$m_{K^*(892)}$	$894.9 \pm 0.5 \pm 0.7$	0.088	0.654	0.660	895.8 ± 0.5
$\Gamma_{K^*(892)}$	$45.7 \pm 1.1 \pm 0.5$	0.148	0.499	0.520	44.2 ± 1.0
$a_{K_0^*(1430)}$ (a.u.)	$1.51 \pm 0.11 \pm 0.09$	-0.024	0.089	0.092	1.76 ± 0.12
$\phi_{K_0^*(1430)}$ (°)	$146 \pm 8 \pm 8$	-0.623	8.442	8.465	145 ± 8
$a_{f_0(980)}$ (a.u.)	$4.72 \pm 0.18 \pm 0.17$	-0.029	0.167	0.170	3.67 ± 0.13
$\phi_{f_0(980)}$ (°)	$157 \pm 3 \pm 4$	-0.343	4.036	4.051	156 ± 3
$a_{\phi(1020)}$ (a.u.)	$1.13 \pm 0.02 \pm 0.02$	0.004	0.017	0.018	1.15 ± 0.02
$\phi_{\phi(1020)}$ (°)	$-8 \pm 4 \pm 4$	0.081	3.850	3.851	-15 ± 4
$a_{f_0(1370)}$ (a.u.)	$1.15 \pm 0.09 \pm 0.06$	-0.003	0.063	0.063	
$\phi_{f_0(1370)}$ (°)	$53 \pm 5 \pm 6$	-0.536	5.820	5.845	
$a_{f_0(1710)}$ (a.u.)	$1.11 \pm 0.07 \pm 0.10$	-0.004	0.098	0.098	1.27 ± 0.07
$\phi_{f_0(1710)}$ (°)	$89 \pm 5 \pm 5$	0.195	4.916	4.920	102 ± 4
FF[$K^*(892)$] (%)	$47.4 \pm 1.5 \pm 0.4$	0.016	0.357	0.4	48.2 ± 1.2
FF[$K_0^*(1430)$] (%)	$3.9 \pm 0.5 \pm 0.5$	0.036	0.460	0.5	5.3 ± 0.7
FF[$f_0(980)$] (%)	$28.2 \pm 1.9 \pm 1.8$	0.096	1.792	1.8	16.8 ± 1.1
FF[$\phi(1020)$] (%)	$42.2 \pm 1.6 \pm 0.3$	0.018	0.277	0.3	42.7 ± 1.3
FF[$f_0(1370)$] (%)	$4.3 \pm 0.6 \pm 0.5$	0.044	0.488	0.5	
FF[$f_0(1710)$] (%)	$3.4 \pm 0.5 \pm 0.3$	0.044	0.311	0.3	4.4 ± 0.4
$\sum_R \mathrm{FF}_R$ (%)	$129.5 \pm 4.4 \pm 2.0$	0.020	1.981	2.0	117.3 ± 2.2
χ^2/ν	178/117				278/119

data. The best improvement is achieved if we add an $f_0(1370)\pi^+$ contribution. We find that a six-resonance model, containing contributions from $K^*(892)^0K^+$, $K_0^*(1430)K^+$, $f_0(980)\pi^+$, $\phi(1020)\pi^+$, $f_0(1370)\pi^+$, and $f_0(1710)\pi^+$ resonances, gives better consistency with our data with $\chi^2/\nu = 178/117$. Tables VII and VIII show that any additional resonance does not have a significant amplitude or fit fraction, or significantly improve the fit quality, and we give upper limits on their fit fractions at the 90% C.L. The fit quality is not excellent and this is mostly caused by a disagreement between the data and the model in the region $1.1 < m^2(K^+K^-) < 1.4\ \mathrm{GeV}^2/c^4$.

In Table IX we show the resonance parameters when they are allowed to float in the fit. We find that the $K^*(892)$ width is 5 MeV/c^2 smaller than in the PDG. This result is consistent with our observation in the $D^+ \to K^-\pi^+\pi^+$ analysis [15]. Other resonance parameters are consistent with their values from the PDG [8] or the BES experiment [13] for $f_0(980)$.

We estimate a systematic uncertainty on fit parameters from numerous fit variations, and Table XIII shows the final results on fit parameters with their statistical and systematic uncertainties.

ACKNOWLEDGMENTS

We gratefully acknowledge the effort of the CESR staff in providing us with excellent luminosity and running conditions. D. Cronin-Hennessy and A. Ryd thank the A. P. Sloan Foundation. This work was supported by the National Science Foundation, the U.S. Department of Energy, the Natural Sciences and Engineering Research Council of Canada, and the U.K. Science and Technology Facilities Council.

[1] P. L. Frabetti *et al.* (E687 Collaboration), Phys. Lett. B **351**, 591 (1995).
[2] J. Alexander *et al.* (CLEO Collaboration), Phys. Rev. Lett. **100**, 161804 (2008).
[3] R. H. Dalitz, Philos. Mag. **44**, 1068 (1953).
[4] A. M. Rahimi, Fermilab Report No. FERMILAB-THESIS-2000-13.
[5] S. Malvezzi, AIP Conf. Proc. **549**, 569 (2000).
[6] G. Viehhauser, Nucl. Instrum. Methods Phys. Res., Sect. A **462**, 146 (2001); D. Peterson *et al.*, Nucl. Instrum. Methods Phys. Res., Sect. A **478**, 142 (2002); Y. Kubota *et al.*, Nucl. Instrum. Methods Phys. Res., Sect. A **320**, 66 (1992); R. A. Briere *et al.* (CESR-c and CLEO-c Taskforces, CLEO-c Collaboration), Cornell University,

LEPP Report No. CLNS 01/1742, 2001 (unpublished).
[7] S. Dobbs *et al.* (CLEO Collaboration), Phys. Rev. D **76**, 112001 (2007).
[8] W.-M. Yao *et al.*, J. Phys. G **33**, 1 (2006).
[9] D. J. Lange, Nucl. Instrum. Methods Phys. Res., Sect. A **462**, 152 (2001).
[10] S. Kopp *et al.* (CLEO Collaboration), Phys. Rev. D **63**, 092001 (2001).
[11] J. M. Blatt and V. F. Weisskopf, *Theoretical Nuclear Physics* (Wiley, New York, 1951), p. 361.
[12] S. M. Flatté, Report No. CERN/EP/PHYS 76-8, 1976; Phys. Lett. **63B**, 224 (1976).
[13] M. Ablikim *et al.* (BES Collaboration), Phys. Lett. B **607**, 243 (2005).
[14] J. A. Oller, Phys. Rev. D **71**, 054030 (2005).
[15] G. Bonvicini *et al.* (CLEO Collaboration), Phys. Rev. D **78**, 052001 (2008).